Proc. Natl. Acad. Sci. USA
Vol. 92, pp. 10954–10958, November 1995
Neurobiology

Particles move along actin filament bundles in nerve growth cones

L. L. EVANS AND P. C. BRIDGMAN

Washington University School of Medicine, Department of Anatomy and Neurobiology, 660 Euclid Avenue, Box 8108, St. Louis, MO 63110

Communicated by Thomas S. Reese, National Institutes of Health, Bethesda, MD, August 18, 1995 (received for review June 29, 1995)

ABSTRACT **Organelle movement along actin filaments has been demonstrated in dissociated squid axoplasm [Kurznetsov, S. A., Langford, G. M. & Weiss, D. G. (1992) *Nature (London)* 356, 722–725 and Bearer, E. L., DeGiorgis, J. A., Bodner, R. A., Kao, A. W. & Reese, T. S. (1993) *Proc. Natl. Acad. Sci. USA* 90, 11252–11256] but has not been shown to occur in intact neurons. Here we demonstrate that intracellular transport occurs along actin filament bundles in intact neuronal growth cones. We used video-enhanced differential interference contrast microscopy to observe intracellular transport in superior cervical ganglion neurons cultured under conditions that enhance the visibility of actin bundles within growth cone lamellipodia. Intracellular particles, ranging in size from <0.5–1.5 μm, moved along linear structures (termed transport bundles) at an average maximum rate of 0.48 μm/sec. After particle movement had been viewed, cultures were preserved by rapid perfusion with chemical fixative. To determine whether particle transport occurred along actin, we then used fluorescence microscopy to correlate this movement with actin and microtubule distributions in the same growth cones. The observed transport bundles colocalized with actin but not with microtubules. The rates of particle movement and the association of moving particles with actin filament bundles suggest that myosins may participate in the transport of organelles (or other materials) in intact neurons.**

Intracellular transport is essential to neuronal function. Cytoskeletal elements, new membrane, and membrane proteins must be continually supplied to specialized regions of the neuronal plasma membrane. The fast component of organelle transport within neuronal processes occurs along microtubule tracks (1, 2). However, microtubules rarely penetrate the cortical actin meshwork that extends beneath the plasma membrane of the entire cell. Therefore, other modes of transport may be required for delivering materials to and from the plasma membrane. *In vitro* studies of organelle motility have shown that axoplasmic organelles are capable of movement along actin filaments (3, 4). We set out to determine whether organelle movement occurs along actin filaments in intact mammalian nerve cells.

The neuronal growth cone, a highly dynamic cellular specialization that guides neurite outgrowth during embryonic development, is ideal for intracellular observations of actin-based organelle movement. The growth cone is a flat, organelle-rich neuronal structure with a well-defined cytoskeleton. Although growth cones exhibit morphological variability, most are characterized by two domains: a thick, microtubule-rich central domain and a thin, actin-rich peripheral domain. We used video microscopy to observe intracellular transport along clearly visible tracks in the periphery of growth cones cultured under conditions that restrict microtubules to the central domain. By following these video observations with fluorescence labeling of cytoskeletal proteins, we show that intracellular particle transport occurs along actin filament bundles in neuronal growth cones.

The publication costs of this article were defrayed in part by page charge payment. This article must therefore be hereby marked "*advertisement*" in accordance with 18 U.S.C. §1734 solely to indicate this fact.

MATERIALS AND METHODS

Materials. Twenty-day, timed-pregnant rats were obtained from Sasco (Omaha, NE). Sympathetic neurons were cultured in C-10-2 medium (5). Monoclonal antibodies raised against β-tubulin were purchased from East Acres Biologicals (Southbridge, MA). Other reagents were cytochalasin B (Sigma), mouse laminin (Collaborative Research), nocodazole (Sigma), and rhodamine–phalloidin (Molecular Probes).

Cell Culture. In preparation for tissue culture, acid-washed, round, glass coverslips (22 mm diameter, no. 0 thickness) were coated with laminin (16 μg/ml in 0.05 M carbonate buffer, 3–6 hr at 37°C) and rinsed thoroughly in L15 medium. Superior cervical ganglion explants were dissected from embryonic day-20 to -21 rat fetuses, desheathed, and cut into approximately eight explants. Explants were then plated in C-10-2 medium/0.5 μM nocodazole. Cultures were grown overnight in a humidified environment with 5% CO_2/95% air at 37°C.

Video Microscopy. For observation of intracellular movements, coverslips were transferred to a perfusion chamber (6) filled with warm Hepes-buffered C-10-2 medium/0.5 μM nocodazole. The chamber was transferred to the heated stage of an inverted microscope equipped for high-resolution, video-enhanced contrast-differential interference contrast (DIC) microscopy. Before each recording, the culture was perfused with warm Hepes-buffered medium/0.5 μM nocodazole/0.5 μM cytochalasin B. Observations of particle movement were made during the first 20 min of cytochalasin treatment. Images from the Newvicon video camera were captured at 5-sec intervals onto optical disk; a real time recording was made simultaneously on magnetic tape. After recording intracellular particle movement, the culture was rapidly perfused with a warm solution of fixative: 0.25% glutaraldehyde/0.1 M cacodylate buffer, pH 7.4/5 mM $CaCl_2$/10 mM $MgCl_2$.

Immunofluorescence. After fixation, coverslips were removed from the perfusion chamber, washed three times in cacodylate buffer, two times in phosphate-buffered saline (PBS), and then permeabilized with 0.02% saponin/PBS/33 nM rhodamine–phalloidin. Coverslips were mounted for microscopy in PBS, pH 8.5/*p*-phenylenediamine at 1 mg/ml to prevent bleaching. Growth cones imaged by DIC microscopy were relocated, and fluorescence images were captured using a cooled charged-coupled-device (CCD) camera (Photometrics CH250; Tucson, AZ). After imaging, coverslips were treated with 1% OsO_4/PBS at 4°C for 5 min, which quenches the glutaraldehyde and removes phalloidin. After being washed five times with PBS, reduced with freshly prepared 5% 2-mercaptoethanol/PBS at 22°C, and blocked in PBS/bovine serum albumin (8 mg/ml)/0.5% fish gelatin/5% normal goat serum, the coverslips were stained with a monoclonal antibody to β-tubulin and a fluorescein-conjugated goat anti-mouse secondary antibody. The coverslips were again mounted for microscopy, and relocated growth cones were imaged with the CCD camera.

Superimposition of DIC and Fluorescence Images. Because DIC and fluorescence images were obtained with different cameras, the DIC image in Fig. 4 was corrected for a slight

Abbreviation: DIC, differential interference contrast.

curvature introduced by the video camera (pincushion effect). To accomplish this, a square-grid pattern was imaged with the Newvicon video camera, and computer algorithms were developed to correct for distortion of the square grid. These algorithms were applied to DIC images that were used in superimpositions with fluorescence images captured with the CCD camera. Fluorescence and DIC images were superimposed by scaling the fluorescence image to the magnification of the DIC image and aligning the images using the cell border and internal geometry of filament bundles.

RESULTS

Adding a Low Concentration of Cytochalasin to Cultures Grown in a Low Concentration of Nocodazole Enhances the Visibility of Cytoskeletal Bundles in the Growth Cone Periphery. The growth cones of rat sympathetic neurons are typically thin and well spread when cultured on laminin substrates; however, the detection of small organelles and individual actin filament bundles within the growth cone periphery is usually difficult and limited to chance observations in exceptionally thin growth cones. Culturing cells under the conditions of this assay produced changes in growth cone morphology that enabled frequent observations of organelle movement along clearly visible bundles in the growth cone periphery.

At the low nocodazole concentration used in these cultures, microtubules continue to polymerize but presumably fail to undergo rapid length changes, as they would in the absence of nocodazole (K. M. Wickline and P.C.B., unpublished results). This alteration in microtubule dynamics produces advantageous changes in growth cone morphology. Growth cones in these cultures have unusually large, extremely thin peripheral domains (Fig. 1 *A* and *B*). Because contrast is improved in DIC images as specimen thickness decreases, these growth cones are optimal for observing intracellular movements using DIC microscopy. Furthermore, the restriction of microtubules to the central domain of the growth cone, which may result from the kinetic stabilization of microtubules under these conditions, facilitates observations of particle movements in microtubule-free regions of the growth cone.

Growth cones cultured in low concentrations of nocodazole are thinner than those cultured without nocodazole, but the density of the cytoplasm within the growth cone periphery often interferes with the ability to distinguish individual actin filament bundles in this region. Therefore, most recordings of intracellular movement were made after addition of medium containing a low cytochalasin concentration. Bundles in the growth cone periphery become well defined after cytochalasin addition (Fig. 1*C*). Presumably, depolymerizing a portion of the actin meshwork within the growth cone increases the difference between the index of refraction of the bundles and that of the surrounding cytoplasm, thereby increasing image

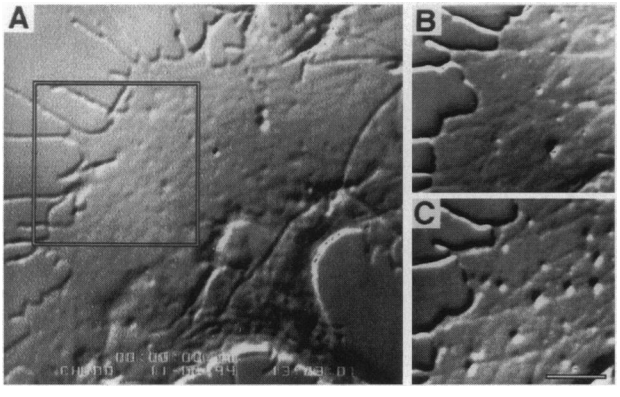

FIG. 1. Adding a low concentration of cytochalasin to cultures grown in a low nocodazole concentration enhances visibility of cytoskeletal bundles in the growth cone periphery. (*A*) Low-magnification view of a growth cone grown in a low nocodazole concentration. (*B*) Higher-magnification view showing the boxed region of the growth cone in *A*. (*C*) Same region shown in *B*, 5 min after addition of a low cytochalasin concentration. (Bar = 5 μm.)

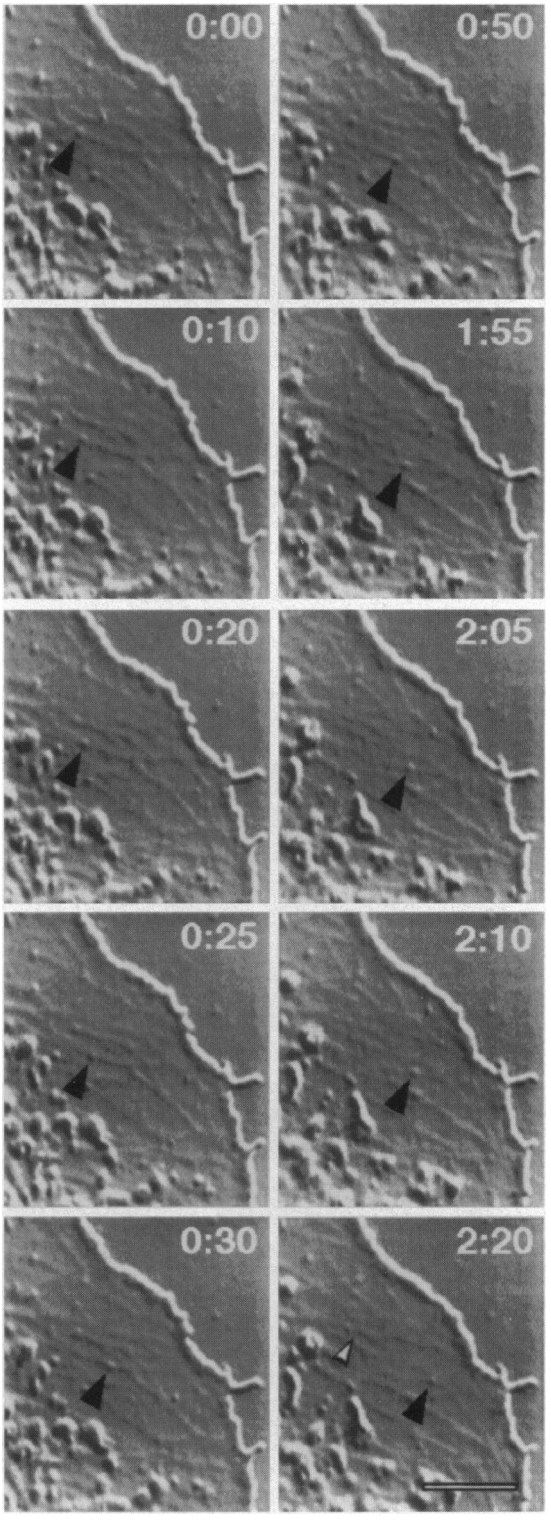

FIG. 2. A high-magnification, time-lapse recording showing particle movement along clearly visible tracks in a growth cone periphery. The particle indicated by the black arrowhead moves along a single bundle, encounters an intersection between bundles, pauses for ≈30 sec, and continues on along another bundle. The 2:20 time point also shows the beginning location (small white arrowhead) of the moving particle. (Bar = 2 μm.)

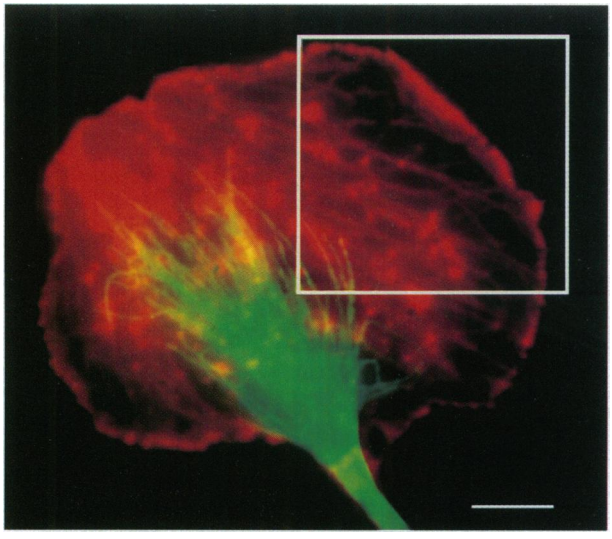

FIG. 3. Actin (red) and microtubule (green) distributions in the growth cone in Fig. 2, shown superimposed at low magnification. The boxed region shows the area in which particle movement was recorded. This growth cone was fixed several minutes after particle movement was recorded. Although the moving particle was not retained in the fixed image, the bundles seen in the live DIC recording remain present in the fixed growth cone. Actin filament bundles, which colocalize with the bundles in the DIC image, are oriented along the axis of particle movement seen in Fig. 2. Microtubules are not oriented in the direction of particle movement and barely extend into the region where particle movement was recorded. (Bar = 5 μm.)

contrast. Few bundles were initially affected by this cytochalasin concentration; however, many bundles deteriorate after ≈30–40 min of cytochalasin treatment. Observations were therefore limited to the first 20 min of treatment. In addition to enhancing image contrast, this treatment also increased the likelihood of observing particle movements, probably because the decreased density of the peripheral cytoplasm allows particles easier access to the growth cone periphery.

Particles Move Along Actin Filament Bundles in the Periphery of Growth Cones. Upon reduction of the thickness and density of the peripheral cytoplasm, intracellular transport was readily seen within the growth cone periphery. Particles, typically <0.5 μm in diameter, moved along clearly visible tracks (bundles) in the growth cone periphery (Figs. 2 and 4*A*). Particles frequently moved into the periphery from the thick, central region of the growth cone, where organelle traffic (presumably microtubule-based) is rapid and abundant. Often, particles moved toward the leading edge of the growth cone opposing the ≈1 μm/min rearward flow of filament bundles and membranous materials from the leading edge of the growth cone (7–9). Retrograde flow from the leading edge opposes this movement; therefore, particle movement along these bundles must be driven by a force-producing protein and could not simply result from the rearward flow of materials from the leading edge. Occasionally particles appeared to fuse with and/or form from the leading edge of the growth cone, indicating that they may participate in recycling membrane or membrane-associated proteins.

Because growth cone morphology is severely disrupted at high concentrations of nocodazole, it is difficult to determine whether intracellular movement in growth cones can occur in the absence of microtubules. Likewise, it is also difficult to determine whether this particle movement continues in the absence of filamentous actin because higher concentrations of cytochalasin also disrupt the thin, well-spread growth cone

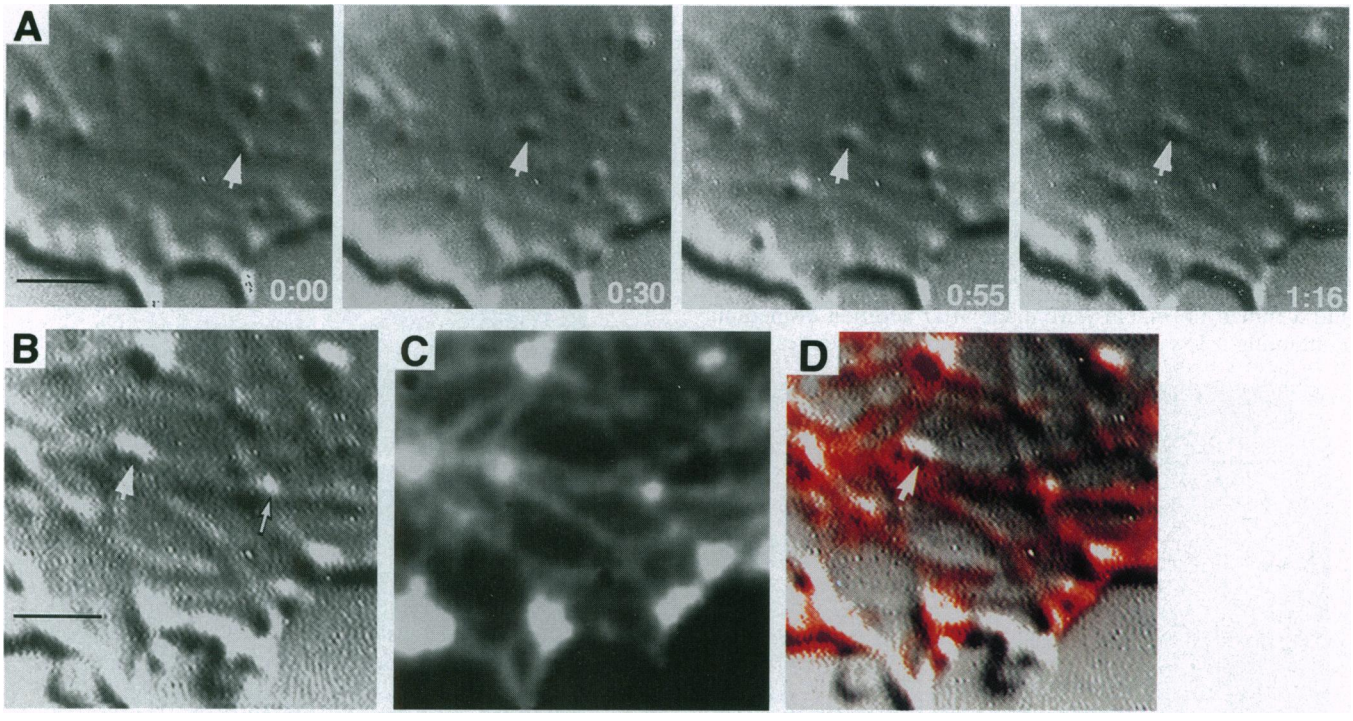

FIG. 4. Moving particles can be immobilized in close apposition to actin filament bundles upon rapid perfusion of glutaraldehyde. (*A*) High-magnification time-lapse recording of particle movement (indicated by arrow) in a growth cone lamellipodia. Fixative was perfused into the culture chamber at time 1:21. (Bar = 3 μm.) (*B*) The same region of growth cone imaged after fixation. This image has been corrected for a slight curvature introduced by the video camera (pincushion effect). Upon fixation, the moving particle (again indicated by large arrow) was retained on the bundle along which it moved. The original position of the particle at time zero is also indicated (small arrow). (Bar = 2 μm.) (*C*) The actin distribution, demonstrated by rhodamine–phalloidin staining, in the same region. The bundles visible in *A* and *B* are actin filament bundles. (*D*) Superimposition of the phalloidin staining with the pincushion effect-corrected DIC image reveals that bright actin foci do not colocalize with the particle (arrow) seen moving along actin bundles in the live image. Although several objects (particles) in the DIC image do colocalize with bright actin foci, these particles did not move during the recording.

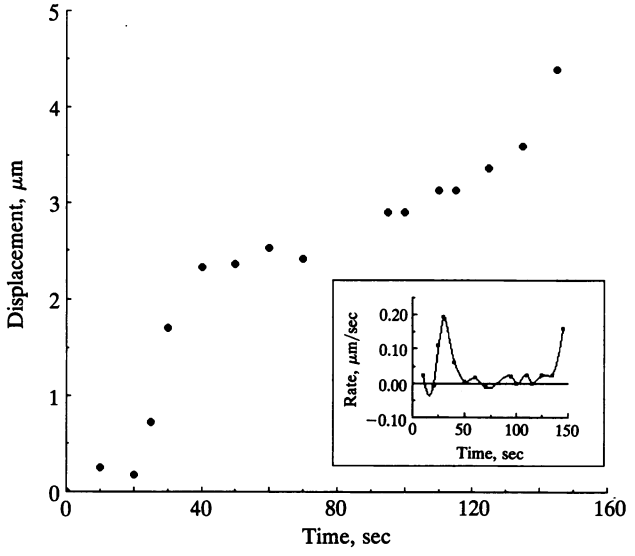

FIG. 5. Displacement analysis of particle movement shown in Fig. 2. Particle displacement in Fig. 2 was measured from its original position at time zero. To correct for field drift, images were aligned with respect to an immobile object on the substratum. Because actin filament bundles in the growth cone periphery move rearward with the retrograde flow, changes in bundle position were accounted for in calculating particle displacement from its original position along a bundle. To accomplish this, the position of the actin filament bundle upon which the particle moved, as well as the particle coordinates, were recorded in each image. Particle coordinates at each time point were then adjusted for changes in bundle position by subtracting the *x,y* coordinates of the bundle shift from the particle coordinates. (*Inset*) Rate of particle movement in Fig. 2 during recording. The first derivative of the displacement versus time plot was used to generate this graph.

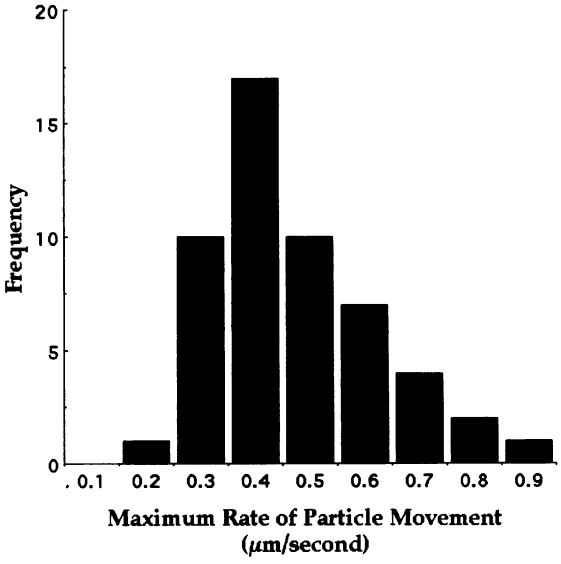

FIG. 6. Histogram showing maximum rates of particle movement. Observations of particle movement in four growth cones were used to calculate the maximum rate of particle movement for 52 separate particles, all of which appeared <0.5 μm in size. As described for previous analyses (Fig. 5), changes in bundle position due to retrograde flow were accounted for in measurement of particle displacement. The maximum displacement for each particle was determined; each maximum displacement value and the time interval during which this displacement occurred were used to calculate the maximum rate of movement for each particle. Maximum rates were grouped into 0.1 μm/sec intervals that center around the rate listed below each category, and the number of observations within each category was recorded. This histogram represents pooled data from observations in four growth cones; the histograms for each separate growth cone show a similar rate distribution.

morphology. Nonetheless, fluorescent labeling of actin and microtubules in fixed samples previously viewed by video microscopy revealed that particle movement recorded in the periphery of these growth cones occurred along actin filaments, not microtubules (Fig. 3). In fact, moving particles were immobilized in close apposition to actin filament bundles in samples rapidly perfused with glutaraldehyde during recordings of particle movement (Fig. 4).

Rates of Actin-Based Intracellular Particle Movement Are Consistent with Myosin-Driven Transport. Understanding the dynamics of intracellular actin-based transport is fundamental to understanding the mechanoenzymes that drive this movement. Therefore, particle displacements along actin bundles in the periphery of growth cones were tracked in time lapse recordings (Fig. 5), and rates of particle movement were calculated. Rates of movement for an individual particle varied, with particles rarely achieving their maximum rate (Fig. 5 *Inset*). These variable rates may result from local differences in cytoplasmic density that influence a particle's ability to move. In fact, rate variations often occurred when particles encountered visible obstacles such as bundle intersections (Figs. 2 and 5, 0:50–1:15) or other particles occupying the same bundle. On rare occasions, moving particles faced with apparently impassable obstacles stopped and reversed direction along a single bundle. If myosins, barbed-end-directed mechanoenzymes, drive this particle movement, then direction reversals on a single actin filament are not possible. However, it is possible that actin filaments of opposite polarity are present in bundles of actin filaments (10). In this case, direction reversals could result when motor enzymes favor an oppositely oriented filament within a bundle.

Observations of particle movement in four growth cones were used to calculate the maximum rate of particle movement for 52 separate particles, all of which appeared <0.5 μm in size (Fig. 6). Most frequently, maximum rates fell in a range between 0.35 and 0.45 μm/sec; however, the mean value of maximum rates, 0.48 μm/sec, is slightly influenced by the few instances where rates reached values between 0.7 and 0.9 μm/sec.

DISCUSSION

We used a specific culture method to consistently visualize intracellular transport along actin filaments in intact neuronal growth cones. Although these culture conditions are not necessary for observations of particle movement along actin bundles, they improve the frequency of observations by enhancing the visibility of actin filament bundles in the growth cone periphery. Our results show that intracellular particles move along actin filament bundles in intact neuronal growth cones.

Although we have clearly observed the transport of small particles along actin filament bundles in intact neurons, the nature of these intracellular particles remains unclear. They may be the small, actin-associated, membrane-bound organelles seen by electron microscopy in the periphery of growth cones cultured in a low concentration of nocodazole and treated with a low concentration of cytochalasin (unpublished results). Alternatively, these particles may be small clusters of cytoskeletal elements or other proteins. The sizes of these particles and the rates of their movement are similar to those of organelles moving along actin filaments in dissociated squid axoplasm (3). This similarity could indicate that these intracellular particles are organelles similar to those seen moving in dissociated squid axoplasm. However, this resem-

blance could also simply reflect a similarity in the motor molecules that drive these types of actin-based movement.

Myosins are the only known actin-based motor proteins. Several lines of evidence suggest that unconventional myosins participate in intracellular transport along actin filaments (4, 11, 12). The rates of actin-based particle movement in growth cones and the association of these particles with actin suggest that myosins participate in this intracellular transport. Interestingly, the rates of this movement are similar to the average rates of *in vitro* actin filament translocation by myosin V (13), an unconventional myosin thought to be involved in organelle movement (12, 13). Myosin V is one of at least two unconventional myosins present in sympathetic nerve growth cones (14).

However, considering the many classes of unconventional myosins, more than one class may be involved in actin-based transport. In fact, recent evidence suggests that more than one type of myosin may be present on organelles from squid axoplasm (4, 15). The variability in maximum rates of actin-based intracellular particle movement and in actin-based organelle movement *in vitro* may reflect this multiplicity. For example, the right-skewed distribution of maximum rates shown in Fig. 6 could represent the superimposition of two rate distributions, each with a slightly different mode and variance. This result could reflect the presence of two populations of particles that are indistinguishable by video microscopy. The difference in these populations could result from the presence of more than one actin-based motor on these particles.

Both the nature of these particles and the type of motor enzymes that drive their movement are uncertain; the function of these intracellular particles also remains unclear. Because microtubules rarely penetrate the cortical actin meshwork, this actin-based transport may be required for delivering materials to and from sites of interaction with the plasma membrane. The delivery of these materials to specialized regions of the neuronal plasma membrane is likely essential for neuronal function; therefore, this actin-based transport may be required for normal nervous system function.

We thank Peter Pletcher for programming and technical assistance, and Drs. John Cooper and Anuradha Rao for valuable discussion and criticism of this manuscript. This work was supported by research grants from the McDonnell Center for Cellular and Molecular Neurobiology and the National Institutes of Health (NS26150).

1. Allen, R. D., Metuzals, J., Tasaki, I., Brady, S. T. & Gilbert, S. P. (1982) *Science* **218,** 1127–1128.
2. Vale, R. D., Schnapp, B. J., Reese, T. S. & Sheetz, M. P. (1985) *Cell* **40,** 559–569.
3. Kuznetsov, S. A., Langford, G. M. & Weiss, D. G. (1992) *Nature (London)* **356,** 722–725.
4. Bearer, E. L., DeGiorgis, J. A., Bodner, R. A., Kao, A. W. & Reese, T. S. (1993) *Proc. Natl. Acad. Sci. USA* **90,** 11252–11256.
5. Johnson, M. I. & Argiro, V. (1983) *Methods Enzymol.* **103,** 334–347.
6. Berg, H. C. & Block, S. M. (1984) *J. Gen. Microbiol.* **130,** 2915–2920.
7. Forscher, P. & Smith, S. J. (1988) *J. Cell Biol.* **107,** 1505–1516.
8. Dailey, M. E. & Bridgman, P. C. (1993) *J. Neurosci.* **13,** 3375–3393.
9. Lin, C.-H. & Forscher, P. (1995) *Neuron* **14,** 763–771.
10. Lewis, A. K. & Bridgman, P. C. (1992) *J. Cell Biol.* **119,** 1219–1243.
11. Mermall, V., McNally, J. G. & Miller, K. G. (1994) *Nature (London)* **369,** 560–562.
12. Cheney, R. E. & Mooseker, M. S. (1992) *Curr. Opin. Cell Biol.* **4,** 27–35.
13. Cheney, R. E., O'Shea, M. K., Heuser, J. E., Coelho, M. V., Wolenski, J. S., Espreafico, E. M., Forscher, P., Larson, R. E. & Mooseker, M. S. (1993) *Cell* **75,** 13–23.
14. Bridgman, P. C., Rochlin, M. W., Lewis, A. K. & Evans, L. L. (1994) in *Progress in Brain Research: Neural Regeneration*, ed. Seil, F. J. (Elsevier, Amsterdam), Vol. 103, pp. 99–107.
15. Cohen, D. L., Kuznetsov, S. A. & Langford, G. M. (1994) *Mol. Biol. Cell*, Suppl. **5,** p. 278a (abstr.).